Flexibility of an Antibody Binding Site Measured with Photon Echo Spectroscopy

Ralph Jimenez, David A. Case, and Floyd E. Romesberg*

Departments of Chemistry and Molecular Biology, The Scripps Research Institute, 10550 N. Torrey Pines Rd., Maildrop CVN22, La Jolla, California 92037

Received: August 10, 2001; In Final Form: October 15, 2001

The lock-and-key and induced fit models of antigen binding by antibodies are topics of considerable importance to immunology and protein biochemistry in general. These models ascribe different degrees of flexibility to the antibody combining site and may therefore be distinguished by measuring the response of the protein to the force exerted by charge redistribution and structural reorganization of an optically excited antigen. Spectroscopic characterization of the magnitude and time scale of this protein reorganization is therefore a basis for comparing the flexibility of different antibodies. This approach is used to study a panel of antibodies elicited to the chromophoric antigen 8-methoxypyrene-1,3,6,trisulfonic acid. The reorganization energies of the chromophore−antibody complexes are determined and are found to be distributed over a wide range. Three pulse photon echo peak shift spectroscopy is used to measure the time scales of the reorganization process in one complex. The antibody motions occur on time scales ranging from 75 femtoseconds to 67 picoseconds. Structural origins of the observed protein motions are discussed.

I. Introduction

The static view of protein structure, which has resulted in large part from the detailed but static view provided by X-ray crystallography, is yielding to a dynamic view of protein structure.[1−3] In this dynamic view, protein motions play an important role in biological function, including protein folding,[4−7] allosteric regulation,[8−12] ligand binding,[13−21] and catalysis.[2,11,12,22−29,30−34] For example, protein fluctuations are well known to play a role in electron transfer reactions by altering the donor and acceptor distances and by allowing the protein to accommodate changes in the substrate or cofactor charge distribution.[35−38] In addition, optimization of ligand binding may require that the protein undergo conformational adjustments. In some cases these conformational adjustments may be delocalized and play an important role in allosteric regulation. Conformational flexibility may also be important during enzymatic catalysis, which typically involves significant atomic displacements or charge reorganization within the enzyme−substrate complex.

The importance of protein flexibility for ligand binding is nowhere more obvious than in the humoral immune system, where a limited set of proteins (antibodies, Ab) must bind a virtually unlimited range of foreign molecules (i.e., small molecule antigens, Ag).[39,40] How the finite set of Ab has such a broad range of specificities is a fundamental question. It has been speculated that conformational diversity of an Ab combining site may allow recognition of multiple Ag, and thus one Ab may provide a suitable starting point for the affinity maturation and somatic evolution of a high affinity Ab against a variety of different Ag.[41] The relative importance of this "induced-fit" mechanism[42,16] versus a "lock-and-key" mechanism,[43,44] where the Ab binding site is rigid and preoptimized for the desired Ag, has been extensively discussed in the literature and is a central issue in immunology,[39,45−47] and more generally, in understanding protein recognition of ligands, cofactors, or substrates.[9,13−15,17,18,48−52]

Crystal structure studies have shown that Ab conformational readjustments upon Ag binding may range from minor adjustments to large scale loop reorganizations.[20,21,39,53] However, these studies reflect static average structures and do not contain dynamic information. For example, an Ab that undergoes large rearrangements might do so by interconverting between two well defined (rigid) structural minima, and therefore such rearrangements may not be interpreted in terms of lock-and-key or induced fit. Dynamic information is necessary. NMR studies may be used to examine the thermal fluctuations about the average structures, and therefore contribute to the characterization of the protein motions.[54−56] However, the observed fluctuations are complex superpositions of all atomic motions, and it has not been possible to use such data to reconstruct specific protein motions. As a result, NMR studies are unlikely to contain sufficient information to distinguish between the lock-and-key and induced fit models.

The differences between these limiting models are manifest neither in the average structures, nor necessarily in the average fluctuation about the average structure. Instead, these models are differentiated in terms of the varying response of a protein to a given force. For example, the combining site of a rigid lock-and-key Ab is expected to respond to a force with high frequency, low amplitude motions, while for a flexible induced-fit Ab, low frequency, large amplitude motions are expected. These low frequency, large amplitude vibrations are the protein motions that allow for structural reorganization that could result in a polyspecific combining site, which is capable of accommodating different ligands. Characterization of the protein response to an applied force, in terms of energies, frequencies, and amplitudes, is now possible with a combination of biology and modern optical spectroscopy. A chromophore may be used to elicit specific and high-affinity Ab from an organism, such as a mouse.[57] The immune system responds as it would to any antigenic compound, by producing high affinity and highly specific Ab that bind the chromophore. The molecular interactions employed by these Ab will be typical of those used by any Ab to bind an Ag and are also likely to be representative of protein interactions with any ligand, cofactor, or substrate. These antibodies may

10.1021/jp013110g CCC: $22.00
Published on Web 01/11/2002

then be isolated and their complexes with Ag spectroscopically characterized.

To characterize protein flexibility, it would be desirable to apply an instantaneous force within the combining site of the Ab and then characterize the resulting motions. Such a force may be applied to the protein by optical excitation of the bound chromophoric Ag. Excitation results in an instantaneous charge redistribution within the ligand, resulting in an Ab−Ag complex that is out of equilibrium. The Ab is therefore under a force until protein motions reestablish equilibrium with the excited chromophore. It is important to emphasize that the protein motions are not photochemically induced, but rather are the protein's response to the altered charge distribution and geometry of the antigen. These protein motions will affect the bound chromophore, in a way that allows for their characterization in terms of their energies, frequencies, and displacements.

The energy of the induced fluctuations is termed the reorganization energy (λ), and is equal to the difference in stability of the Ab complex with the antigen in its ground and excited electronic states.[58] As such, λ is a thermodynamic quantity, but it is related to the dynamic aspects of the fluctuations, i.e., the frequencies (ω_j) and dimensionless displacements (Δ_j) of the vibrations involved for a single or for multiple harmonic vibrations, by the following equations.

$$\lambda_j = \frac{1}{2}\omega_j\Delta_j^2$$

and

$$\lambda_{\text{total}} = \sum_j \frac{1}{2}\omega_j\Delta_j^2 \qquad (1)$$

A full characterization of induced protein fluctuations is included in these equations. λ_{total} may be readily calculated from steady-state absorption and emission spectra.[59,60] The experimental challenge is then to partition the reorganization energy into its constituent modes and to measure ω_j, which then uniquely determine Δ_j. Recently, time-resolved nonlinear optical techniques, such as photon echo spectroscopy, have been used to determine the time scales and amplitudes of fluctuations that affect chromophore electronic states.[61−64] Mukamel has developed a theoretical framework unifying the various spectroscopic techniques and has presented methods for analyzing the experiments in terms of the underlying dynamics.[65] The three pulse photon echo peak shift (3PEPS) experiment has been used,[62,66−73] most notably by Fleming and co-workers, to study solvation dynamics in liquids,[74−79] glasses,[80,81] and proteins.[60,82−85] The peak shift decay time scales and amplitudes may be fit with a model based on the set of nuclear motions coupled to the fluctuations of the S_0-S_1 electronic energy gap of the chromophore.[65,79] The spectral density of these motions characterize the frequencies and amplitudes of all chromophore and protein vibrations. X-ray structural data, along with molecular dynamics simulations, will then be used to determine the molecular origins of the protein motions. In this manner, the conformational flexibility of the protein may be determined. Moreover, a comparison of multiple Ab−Ag complexes will quantitate the contributions of induced-fit and lock-and-key mechanisms of Ag recognition within a given immune response.

A family of high-affinity IgG Ab that bind the chromophore 8-methoxypyrene-1,3,6-trisulfonate (MPTS, Figure 1) have been isolated from mice.[57] These IgG Ab are heterodimeric proteins (~150 KDa) that have two Ag binding sites per molecule.[39,40,86] The absorption and emission spectra of the Ab−MPTS complexes are reported and used to calculate the λ_{tot}, which quantitates the energetics of the combining site fluctuations. The 3PEPS experiment is then used to determine the time scales of the motions in one Ab−MPTS complex. The 3PEPS data is fit with a complete model spectral density that contains both environmental (solvent or protein) and MPTS vibronic structure. This procedure allows for the accurate characterization of both protein and cofactor motions, including those on an ultrafast (sub-100 fs) time scale.

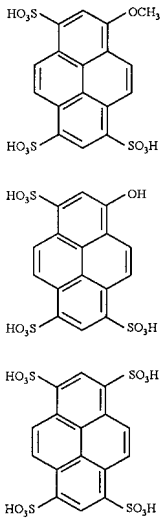

Figure 1. Molecular structures of MPTS (top), HPTS (center), and PTS (bottom).

II. Experimental Section

A. Laser System and Optical Arrangement. The ultrafast laser source used in these measurements is a Ti:sapphire regenerative amplifier system. The seed source, which gives sub-20 fs pulses tunable from 780 to 840 nm, is a home-built Kerr lens mode-locked Ti:sapphire oscillator pumped by the second harmonic of a CW diode-pumped Nd:YVO_4 laser (Spectra Physics Millenia). The seed pulses are amplified in a Spectra Physics sub-50 fs Spitfire amplifier, pumped by a diode-pumped Nd:YLF (Evolution II) at a repetition rate of 5 kHz. The compressed output consists of 40−50 fs pulses with energies of 160−170 μJ.

A beam containing approximately 20% of the amplifier pulse energy is reduced in diameter ~1.5-fold with a telescope, then doubled in a 0.1 mm, Type I LBO crystal. The second harmonic pulses (s-polarized) are separated from the fundamental (p-polarized) with a dichroic beam splitter and compressed by double-passing a pair of Brewster-angled fused silica prisms before entering the experimental setup. The beam is split into three equal portions with beam splitters. One pulse ($\mathbf{k_1}$) travels a fixed delay, whereas the other two pulses ($\mathbf{k_2}$ and $\mathbf{k_3}$) travel variable delays controlled by retroreflecting mirrors mounted on DC motor-controlled linear stages with linear encoder feedback (Kensington Laboratories, PM6000). These linear positioners give step sizes and repeatability of 2 fs, which was found to be essential for reproducibility of the peak shift measurement. The three beams were arranged in an equilateral triangle of ~7 mm per side, which was focused into the sample cell with a 300 mm focal length plano-convex fused silica lens. It was found to be more critical for the reproducibility of the blue light 3PEPS measurement, as compared to longer wavelength experiments, that the triangle is undistorted over several

meters. After the sample cell, another fused silica lens collimated the beams. The 3PEPS and transient grating (TG) signals, in the phase-matched directions $\mathbf{k_1}-\mathbf{k_2}+\mathbf{k_3}$ and $-\mathbf{k_1}+\mathbf{k_2}+\mathbf{k_3}$, were detected with large-area avalanche photodiodes (Advanced Photonix). A phase-locked chopper (New Focus #9801), synchronized to the Q-switch of the regenerative amplifier, chopped beam $\mathbf{k_1}$ at half the repetition rate. Two lock-in amplifiers (Stanford SR830) referenced to the chopper frequency were used to sample the output of the detectors. For the 3PEPS experiment, the coherence period τ (delay between $\mathbf{k_1}$ and $\mathbf{k_2}$) is scanned from negative to positive delays, for fixed values of T (delay between $\mathbf{k_2}$ and $\mathbf{k_3}$), to find the maximum of the integrated signal. The temporal shift of the maximum from zero delay is referred to as the peak shift. For transient grating measurements, pulses $\mathbf{k_1}$ and $\mathbf{k_2}$ are overlapped, and $\mathbf{k_3}$ is scanned.

The excitation wavelengths ranged from 400 to 403 nm, depending on the experiment, with spectral fwhm of 6−7 nm. Since nonlinear crystals such as BBO are not available for harmonic generation of this wavelength range, the pulse width was found by fitting the rising edge of transient absorption signals of cytochrome *c*, and of aqueous MPTS, both of which are assumed not to have any rise times intrinsic to their dynamics. Pulse widths of 35−40 fs fwhm were usually determined. The time overlap of the three pulses for the 3PEPS measurement was achieved by adjusting the delays of $\mathbf{k_2}$ and $\mathbf{k_3}$ so that the two symmetrically related two pulse echo signals formed by each of the two beams with $\mathbf{k_1}$ cross at zero. One advantage of this procedure is that it may be used on the experimental sample itself.

B. Sample Preparation. The succinimidyl ester of MPTS was obtained from Molecular Probes (Eugene, OR), and KLH (keyhole limpet hemocyanin) conjugates were prepared according to the manufacturer's protocols. The conjugate was then purified by size-exclusion chromatography. The KLH-MPTS conjugate was injected into Swiss Webster mice, and monoclonal antibodies were produced and purified from hybridoma supernatants by standard methods.[57] Nineteen anti-MPTS Ab were isolated and stored at 4 °C in 50 mM PBS buffer (pH 7.4). Sodium azide was added to ensure sterility.[57] MPTS and 1,3,6,8-pyrenetetrasulfonic acid (PTS) were obtained from Molecular Probes, and 8-hydroxy-1,3,6-pyrenetetrasulfonic acid (HPTS) was obtained from Aldrich. All were used without further purification. HPLC grade solvents were purchased from Aldrich.

Absorbance spectra were measured in 1 cm quartz cells with a Cary 300 Bio spectrophotometer used in double-beam mode at 2 nm resolution, with 1 nm steps and 0.5 s/point averaging. Mixtures of the Ab and MPTS (10 μM antibody, 16 μM MPTS in 50 mM pH 7.4 PBS buffer) were placed in the sample beam, while antigen-free solutions (10 μM antibody in 50 mM pH 7.4 PBS buffer) were used as a reference in order to subtract contributions from the protein absorption centered at 280 nm. Fluorescence spectra were measured in 1 cm quartz cuvettes using a SPEX fluorolog fluorimeter with 1 nm excitation bandwidth, 2 nm detection bandwidth, and 0.5 s/point averaging, except for measurements on MPTS 5D11 and 10A6, which required 4 s/point averaging. Control experiments using Ab of different specificities were performed to ensure that the observed spectral features resulted from specific Ab−Ag interactions. Numerical processing was performed with PC-based data analysis software. Absorption and emission spectra were baseline corrected and normalized, then numerically integrated with a trapezoidal integration method. The reorganization energies were calculated with eq 2 for 13 anti-MPTS Ab. Error in the reorganization energies (±5%) resulted from noise in the emission spectra and the quality of subtraction of the protein absorbance at short wavelengths. Experimentally measured spectra were converted from nm (wavelength) to cm^{-1} (energies) by multiplying the ordinate values by the wavelength squared, then inverting the abcissa values and multiplying by 10^7.[87] Peak energies were determined by choosing the maximum point from a 1 cm^{-1} step size, cubic spline fit of each spectrum. Competitive ELISAs were used to demonstrate specificity and high affinity of each monoclonal Ab.[86]

Samples for 3PEPS were prepared by concentrating dilute (1.5 mg/mL) solutions of Ab with 30 000 MWCO filtration units (Amicon) to 500 μM, then adding 0.8 equivalent of MPTS per binding site. The sample concentrations were adjusted to give an absorbance of 0.5−0.6 at the excitation wavelength. Protein samples were in 50 mM PBS buffer, pH 7.4. In all cases below, MPTS in aqueous solution or buffer refers to MPTS in the same buffer solution used for the protein studies. A homemade fused-silica spin cell, which uses volumes of ~150 μL (250 μm path length), was used to spin the samples at approximately 1000 rpm. Pulse energies of 2 to 10 nJ per beam were used. Pulse energies of more than 20 nJ per beam had no effect on the shape of the signals.

III. Computational Methods and Models

A. Calculation of Reorganization Energies from Measured Spectra. If the shapes of the absorption and emission spectra are Gaussian, the reorganization energy is equal to half of the Stokes shift ($\omega_{abs} - \omega_{fluor}$). However, when the spectral shapes are not Gaussian, this simple relationship underestimates the reorganization energy. Since MPTS shows a highly structured absorption spectrum, a more sophisticated approach is required. Recently, Jordanides et al. have derived a more general relationship between the experimental spectra and the reorganization energy:[60]

$$\lambda_{total} = \hbar \frac{\int_0^\infty \tilde{\omega}[\sigma_a(\tilde{\omega}) - \sigma_f(\tilde{\omega})]\, d\tilde{\omega}}{\int_0^\infty [\sigma_a(\tilde{\omega}) + \sigma_j(\tilde{\omega})]\, d\tilde{\omega}} \qquad (2)$$

where $\sigma_a(\omega)$ and $\sigma_f(\omega)$ are the absorption and fluorescence line shapes, and $\tilde{\omega}$ is the frequency axis shifted by the crossing frequency ω_{eg} of the absorption and emission spectra ($\omega - \omega_{eg}$). In addition to being a fundamental property of a system that describes the fluctuation thermodynamics, the reorganization energy is also useful in modeling the 3PEPS data, as described below.

B. Modeling of 3PEPS Data. In the most commonly employed description of the TG and 3PEPS signals, the molecular system is modeled with a ground state (S_0) and a single excited electronic state (S_1).[59,65] Nuclear dynamics determine the width and shape of the absorption spectrum by causing fluctuations of the (S_0-S_1) energy gap. The starting point for the calculation of the nonlinear signals is the spectral density, $\rho(\omega)$, which characterizes the distribution of time scales of fluctuations coupled to the electronic transition. The spectral density contains contributions both from solvent or protein fluctuations as well as chromophore vibrational motions. The relative weight of each contribution is scaled by its reorganization energy, λ, and coupling strength, $\langle\delta^2\rangle$. Spectral dynamics of the system are contained within the line broadening function, $g(t)$, which may be calculated from $\rho(\omega)$ by the expression

$$g(t) = i\int_0^\infty d\omega\rho(\omega)\sin(\omega t) + \int_0^\infty d\omega\rho(\omega)\coth\left(\frac{\hbar\beta\omega}{2}\right)[1-\cos(\omega t)] + \frac{(\Delta_{in}t)^2}{2} \quad (3)$$

in which Δ_{in} is the inhomogeneous broadening, $\beta = 1/(k_BT)$, k_B is the Boltzmann constant, and T is the absolute temperature. The term $\rho(\omega)$ is scaled by its first and second moments,

$$\lambda_i = \hbar\int_0^\infty d\omega\omega\rho_i(\omega) \quad (4)$$

$$\langle\delta_i^2\rangle = \int_0^\infty d\omega\omega^2\coth\left(\frac{\hbar\beta\omega}{2}\right)\rho_i(\omega) \quad (5)$$

which are the reorganization energy and coupling strength, respectively. Solvent contributions to $\rho(\omega)$ are incorporated as either Gaussian,

$$\omega^2\rho(\omega) = \frac{\lambda}{\sqrt{\pi}}\left(\omega\tau_g\exp\left[\frac{-(\omega\tau_g)^2}{4}\right]\right) \quad (6)$$

or Lorentzian,

$$\omega^2\rho(\omega) = \frac{\lambda}{2\pi}\left[\frac{2\omega\tau_e}{1+(\omega\tau_e)^2}\right] \quad (7)$$

functions in which τ_g and τ_e are Gaussian and exponential decay times. The absorption spectrum may then be calculated according to

$$\sigma_a(\omega) = \frac{1}{\pi}\mathrm{Re}\int_0^\infty dt\exp[i(\omega-\omega_{eg})t - g(t)] \quad (8)$$

Signals for the various time-resolved experiments such as transient absorption, transient grating, or 3PEPS may be calculated by inserting $g(t)$ into the appropriate response functions, R_1-R_8, selected by the particular measurement.[65,78] The experimentally observed signal in the direction $-\mathbf{k_1}+\mathbf{k_2}+\mathbf{k_3}$ is then proportional to the square of the third-order polarization, which is calculated by convolution of the response functions with the optical fields ($\mathbf{E}_i(\boldsymbol{k}_i,t_i)$, where $\boldsymbol{k}_i$ and t_i are the wavevectors and interaction times) of the experimental pulses:

$$P^{(3)}(\tau,T,t') \propto \int_0^\infty dt'_3\int_0^\infty dt'_2\int_0^\infty dt'_1\sum_{i=1}^{8}R_i(t'_1,t'_2,t'_3)\mathbf{E}_1^*(\mathbf{k}_1,t_1)\mathbf{E}_2(\mathbf{k}_2,t_2)\mathbf{E}_3(\mathbf{k}_3,t_3) \quad (9)$$

This description applies to a system in which coherence is created within a two level system, so that dynamics may be followed as long as there is population in the excited state. In this case, the longest measurable time scales are therefore limited by the excited state lifetime. However, in the more general case of a third, dark state, the ground state recovery time will limit the temporal range of the 3PEPS measurement.

C. Quantum Chemical Methods. Detailed information on chromophore vibrations is useful for fitting the shape of the absorption spectrum and the 3PEPS signal. For the latter, inclusion of intramolecular modes influences both the magnitude of the initial peak shift and the wavelength dependence of the peak shift decay. The intramolecular portion of the spectral density may be determined with resonance Raman spectroscopy.[63,88,89] However, it was not possible to observe any resonance Raman scattering from solutions of MPTS. Thus, quantum chemistry calculations were used to estimate the mode-specific reorganization energies.

The theory of resonance Raman intensities and charge-transfer reorganization energies is complex,[89] but tractable computations are possible with the harmonic approximation and the assumption that the ground and excited state surfaces have different equilibrium geometries but the same vibrational frequencies. Mode-specific reorganization energies and estimates of Raman intensities may then be readily determined from the calculated ground state vibrational frequencies and the geometry change upon excitation.[90,91] By projecting each mode onto the ground/excited state geometry change, one can determine a dimensionless displacement Δ. From this, the reorganization energy is obtained from eq 1.

There are a variety of ways to obtain good estimates of ground state geometries and vibrational frequencies for conjugated systems such as pyrene and the substituted versions considered here. However, obtaining a good description of the optically allowed excited state is more difficult. Qualitatively, this system can be considered in terms of a four-orbital model, with strong mixing among the configurations that can be created from excitations out of two occupied orbitals into two unoccupied orbitals. This leads to a strongly allowed transition (polarized along the long axis of the molecule) and a nearly forbidden state (polarized along the short axis). Neither state can be even approximately represented as a single configuration built from molecular orbitals. The single-excitation configuration interaction (CIS) model is one of the few techniques that can represent strongly mixed states, can be used for geometry optimization, and can be routinely applied to molecules of the size of MPTS. Although vertical excitation energies are generally overestimated, the CIS method appears to give a good account of excited state geometries for molecules of this type.[92] Goodpaster et al.[93] have reported extensive results on the core pyrene system at the level of theory used here (CIS/6-31G*). Furthermore, Mroginski et al. have recently shown that this level of theory is sufficient to simulate resonance Raman spectra.[91]

The ground state wave function that most closely corresponds to the CIS description of the excited state is a Hartree−Fock (HF) single configuration. Hence, we have compared HF and CIS geometries in order to estimate the geometry change upon excitation. The anionic and protonated forms of MPTS were examined (overall charges of −3 and zero, respectively) and only minor differences were found. For comparison, density functional theory (DFT, B3LYP) with a 6-31G* basis set was also used, where frequency errors are generally considerably smaller, to calculate the MPTS ground-state frequencies. Since both methods are known to overestimate vibrational frequencies, the results of a ground state frequency calculation for pyrene were compared with an experimental Raman spectrum[100] in order to derive an overall multiplicative scaling factor for the calculated frequencies. Values of 0.92 and 0.97 were found for the HF and DFT calculations, respectively. These scaling factors were used for MPTS in all the simulations described below. However, errors caused by uncertainties in the ground state vibrational frequencies are probably quite minor: reliance on a CIS excited state geometry, use of gas-phase results for the interpretation of condensed phase measurements, and adoption of a simple harmonic model for reorganization are larger sources of uncertainties in the computed results. Despite these limitations, the quantum results can provide useful information about mode-specific reorganization of the chromophores that is difficult to obtain by other methods.

TABLE 1: Solvent Spectral Data

chromophore/solvent	ω_{abs} (cm^{-1})	ω_{fluor} (cm^{-1})	ω_{eg} (cm^{-1})	σ_{0-0} (cm^{-1})	λ (cm^{-1})
MPTS/water	24755	23200	24118	500	2097
MPTS/EtGly	24811	23849	24431	380	1857
MPTS/MeOH	25045	24024	24584	330	2081
MPTS/EtOH	25070	24404	24805	300	1873
MPTS/DMSO	25144	24441	24868	275	1955
MPTS/MeCN	25273	24829	25098	290	1809
HPTS/water	24774	22429	23919	550	2343
HPTS/EtGly	24653	23209	24105	450	2088
HPTS/MeOH	24814	23673	24392	400	2034
HPTS/EtOH	24814	23853	24406	400	1987
HPTS/DMSO	24935	24248	24664	340	1905
HPTS/MeCN	25157	24550	24936	330	1947
PTS/water	26642	26032	26433	320	1456
PTS/EtGly	26494	26032	26330	309	1443
PTS/EtOH	26617	26041	26450	305	1431
PTS/DMSO	26457	26087	26324	301	1385

All calculations were carried out with the Gaussian 98 suite of programs.[94] The Opt = Tight option was used to obtain accurate geometry optimized structures for the ground and excited states. Dimensionless displacements were computed for each ground state normal mode:[90]

$$\Delta_s = 0.171\tilde{\nu}^{1/2}\sum_j L_{sj}\Delta r_j \qquad (10)$$

Here L_{sj} is the component of normal mode s along Cartesian direction j, Δr_j is the displacement between the ground and excited states, and $\tilde{\nu}$ is the frequency. The constant 0.171 is appropriate if the frequency is expressed in cm^{-1} and the normal mode displacements in Å. Coupling strengths are then found from[80,74]

$$\langle\delta_j^2\rangle = \frac{2\lambda_j\omega_j}{e^{\beta\hbar\omega_j}-1} + \frac{1}{2} \qquad (11)$$

and the vibrational spectral density function ($\rho_{MPTS}(\omega)$) is the sum over all modes

$$\rho_{MPTS}(\omega) = \sum_j \frac{2}{\pi}\frac{\omega^{-2}\tanh(\hbar\beta\omega/2)\langle\delta_j^2\rangle}{(\omega_j^2-\omega^2+\Gamma_j^2)^2+4\omega^2\Gamma_j^2}[\Gamma_j^3+\omega^2\Gamma_j+\omega_j^2\Gamma_j] \qquad (12)$$

where $1/\Gamma_j$ is the damping time for each mode, and all other variables are as defined above.

IV. Results

A. Solvent Studies of MPTS: Absorption Spectra, Emission Spectra, and Reorganization Energies. A detailed understanding of the solvation dynamics of MPTS is required before the chromophore may be used as a probe of antibody dynamics. Therefore, a thorough investigation of the spectroscopy of MPTS in a variety of solvents was performed. Solvent studies were also used to characterize the related molecules HPTS and PTS (Figure 1), to interpret the MPTS data.

(i) Absorption and Emission Spectra. The effect of solvent polarity was examined by measuring the absorption and emission spectra of MPTS, PTS, and HPTS in water, methanol, ethanol, ethylene glycol, dimethyl sulfoxide (DMSO), and acetonitrile (Table 1 and Figure 2). A red-shift (518 cm^{-1}) in absorption energy (ω_{abs}) of MPTS was observed with increased solvent polarity (acetonitrile versus water), which indicates an increased dipole moment in the excited state relative to the ground state.[58] This result is supported by molecular orbital calculations (see below). A similar red-shift was observed for HPTS with increasing solvent polarity (500 cm^{-1}), but a small blue-shift (185 cm^{-1}) was observed for PTS. The shapes of the MPTS and HPTS absorption spectra are solvent dependent as the width (standard deviation, σ_{0-0}) of the lowest energy peak in the spectra of both chromophores increased with increasing solvent polarity. The PTS absorption spectrum broadened slightly with increased solvent polarity. The fluorescence spectra of each chromophore were not mirror images of the corresponding absorption spectra, indicating that substantial changes in vibrational frequencies occur upon excitation. The PTS emission maximum showed little solvent dependence (shifting by no more than 55 cm^{-1}), while for both unsymmetrical chromophores, ω_{fluor} red-shifted with increasing solvent polarity (1629 and 2121 cm^{-1} for MPTS and HPTS, respectively). A correlation between σ_{0-0} and ω_{eg} and ω_{fluor} for both MPTS and HPTS implies that the low frequency spectral features of both chromophores are predominantly broadened by solvent, rather than by chromophore vibrations. This interpretation is supported by quantum chemistry calculations for MPTS, which demonstrated that only 8.7% of the vibrational reorganization energy involves modes with frequencies lower than 1000 cm^{-1}.

(ii) Solvent Dependence of MPTS Reorganization Energy. Reorganization energies were calculated using eq 2 and are listed in Table 1. The reorganization energies were solvent dependent, again with the smallest effects for PTS (which shows a 70 cm^{-1} shift with varying solvents) and larger effects for MPTS and HPTS (288 and 438 cm^{-1}, respectively). Values for MPTS λ_{total} ranged from 1809 cm^{-1} in acetonitrile to 2097 cm^{-1} in water. For MPTS, the reorganization energy is not correlated with ω_{abs}, ω_{fluor}, σ_{0-0}, nor is it correlated with solvent dipole moment, dielectric constant, polarizability, or π^* polarity scales. For HPTS (in the protonated form) a smooth correlation was apparent between λ and ω_{abs}, ω_{fluor}, σ_{0-0}.

The magnitudes of the reorganization energies are on the order of those observed for coumarins[95,96] but significantly larger than those observed for xanthene dyes.[77,97] This result is at first surprising considering the apparent rigidity of the MPTS pyrene framework and the small change in dipole moment upon excitation. As discussed below, the majority of this reorganization results from MPTS vibronic structure.

B. Absorption Spectra, Emission Spectra, and Reorganization Energies of Ab−MPTS Complexes. *(i) Absorption and Emission Spectra of Ab−MPTS Complexes*. Steady-state spectra of the Ab−MPTS complexes were examined. The absorption spectra for the anti-MPTS Ab with bound MPTS are shown in Figure 3. The values of ω_{abs} and ω_{fluor} are listed in Table 2. All of the antibody combining sites shift ω_{abs} of MPTS to lower

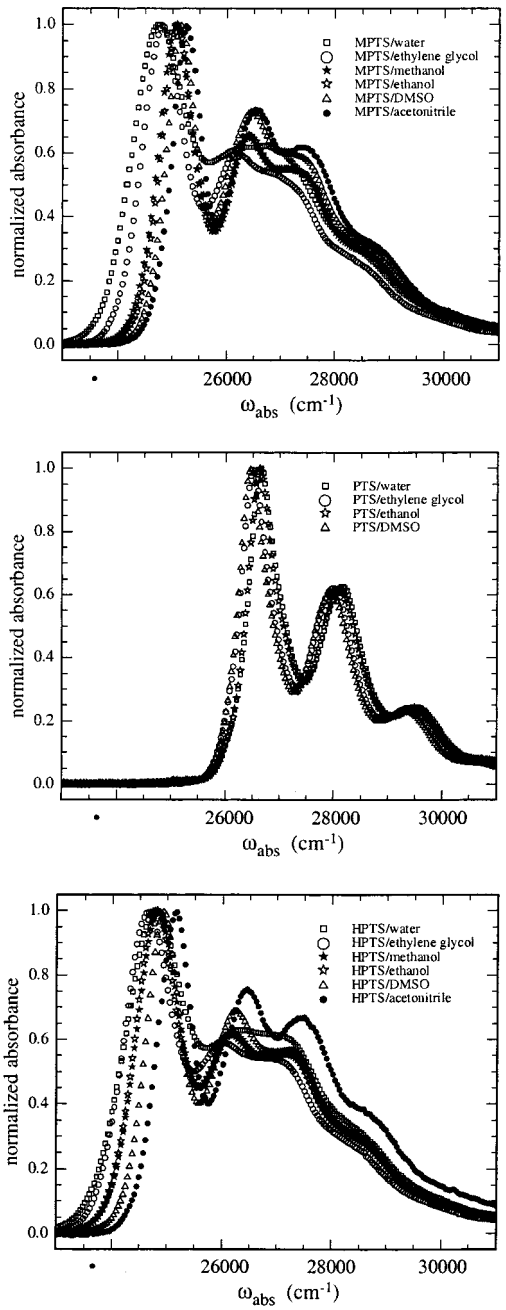

Figure 2. Absorption spectra of MPTS (top), PTS (center), and HPTS (bottom) in solvents.

energies by 45 to 590 cm^{-1} relative to the aqueous value. Two Ab, 5D11, and 10A6 show dramatically altered spectral line shapes, which are similar to those observed for pyrene−paraquat charge transfer complexes in micelles.[98] Binding of MPTS to the other anti-MPTS Ab was less perturbative, causing only red-shifts and small changes in spectral shape and width. The emission of MPTS was strongly quenched (~90%) by the following Ab: 3D3, 9D5, 10A6, 5D11, 4B2, 4F4, 2E8. The MPTS emission bands, like the absorption bands, were typically shifted to higher frequencies (Table 2) and showed increased structure, especially in cases where the corresponding absorption spectra were narrow. The emission spectra of 5D11 and 10A6 showed broad, low intensity, long wavelength bands most likely resulting from charge transfer.

(ii) Reorganization Energies of Ab−MPTS Complexes. The reorganization energies for MPTS bound to the 13 Ab were all reduced relative to aqueous solvation and vary from 1555 to

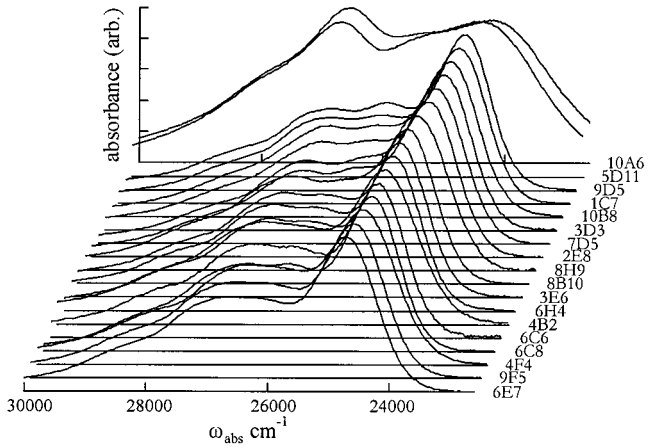

Figure 3. Absorption spectra of MPTS−Ab complexes. MPTS forms tight (nM affinity) complexes with each Ab. The spectral distortions evident in the complexes with Ab 10A6 and 5D11 likely result from charge transfer (see text).

TABLE 2: Spectral Properties of MPTS−Ab Complex

Ab	ω_{abs} (cm^{-1})	ω_{fluor} (cm^{-1})	ω_{eg} (cm^{-1})	σ_{0-0} (cm^{-1})	λ (cm^{-1})
6C8	24649	23581	24172	450	1910
3D3	24424	23272	23975	440	1612
3E6	24593	23553	24115	440	1864
4B2	24621	23159	24059	510	1842
8H9	24537	23244	24003	495	1880
6C6	24621	N/A	N/A	430	N/A
1C7	24396	N/A	N/A	440	N/A
5D11	24256	23216	23778	950	1592
6H4	24593	23525	24115	440	1843
7D5	24450	23328	23947	465	1753
10A6	24161	24528	24925	900	1632
2E8	24453	23413	24031	445	1555
8B10	24587	N/A	N/A	460	N/A
9F5	24691	N/A	N/A	490	N/A
4F4	24649	23244	24087	520	1815
9D5	24395	23369	N/A	400	N/A
10B8	24445	N/A	N/A	450	N/A
6E7	24706	23160	24115	495	1960

1991 cm^{-1} with an average value of 1782 ± 142 cm^{-1}. The smallest reorganization energies (<1632 cm^{-1}) were observed with Ab 2E8, 5D11, 3D3, and 10A6. The largest reorganization energies were observed for Ab 6C8 and 6E7. The Ab−MPTS reorganization energies are not correlated to ω_{abs} or ω_{eg}. Unlike the behavior of MPTS in the various solvents, σ_{0-0} is not correlated to ω_{abs} or ω_{fluor} in the Ab combining sites.

C. Transient Grating Measurements. Transient grating measurements were performed on MPTS in water, ethanol, and Ab 6C8 to determine the excited state lifetimes as well as the frequencies of any underdamped vibrations of the chromophore. We were particularly interested in any changes in chromophore vibrations upon Ab binding. TG signals were fit to the functional form

$$I(t) = \sum_i a_i e^{-t/\tau_i} + \sum_j b_j e^{-t/\tau_{damp,j}} \cos(\omega_j t + \phi_j) \qquad (13)$$

The data are shown in Figure 4, and fit results are summarized in Table 3. Long time scale (200 ps) scans showed no appreciable decay for MPTS in the various solvents, indicating a very long excited state lifetime. However, in Ab 6C8, a decay time scale of 184 ps was observed, which likely corresponds to an excited state lifetime that is dramatically shortened relative to the unbound lifetimes. This interpretation is consistent with

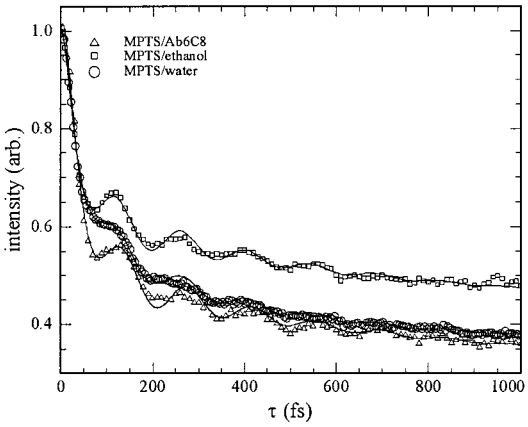

Figure 4. Transient grating measurements and fits for MPTS in water, ethanol, and Ab6C8. Fit parameters are collected in Table 3.

TABLE 3: Fit Parameters for Transient Grating Data

solvent	a_1	τ_1 (fs)	a_2	τ_2 (fs)	a_3	τ_3 (ps)	b_1	ω (cm^{-1})	τ_{damp} (fs)	ϕ
ethanol	0.73	34	0.18	470	0.47	22	0.07	235	250	0.74
water	0.62	48	0.22	325	0.47	22	0.085	229	140	0.8
Ab6C8	1.31	30	0.21	400	0.47	22	0.05	235	370	0.34

significant fluorescence quenching of the chromophore when bound to Ab 6C8. A single underdamped oscillation was apparent in each TG decay. In the various solvents, this vibration must correspond to in-plane motion due to symmetry restrictions. The observed frequency (230 cm^{-1}) and damping time (250 fs) were largely invariant in each solvent or Ab. This insensitivity implies that MPTS does not undergo dramatic structure alterations in the different environments. The damping time is short compared to the 2 to 3 ps dephasing times expected for a ground state vibration. This frequency may therefore correspond to a superposition of multiple vibrations of commensurate frequency in the ground state. Alternatively, the oscillation may be due to an excited state vibration, which is typically thought to undergo faster dephasing than ground state motions.

D. 3PEPS in Solvents and Ab 6C8. 3PEPS decays for MPTS in water, DMSO, ethanol, and Ab 6C8 are shown in Figure 5. Parameters for exponential fits to these data are tabulated in Table 4. Although a quantitative discussion of the relaxation time scales requires modeling with a spectral density, simple exponential fits to the 3PEPS decays accurately represent dynamics on time scales longer than the bath correlation time.[79,66] The initial peak shift in the DMSO 3PEPS experiment is much larger (23 fs) than for the other solvents or Ab 6C8 (10−12 fs). Since the initial peak shift is inversely proportional to λ_{total}, this indicates that the total reorganization energy is smaller in DMSO than the other solvents. In each environment, MPTS shows similar fast (20−40 fs), large amplitude (50−80% of total) decay, followed by slower components of variable time scales. The water data was well fit with a biexponential function, whereas the remaining solvent and Ab 6C8 data required three exponential decays. The Ab peak shift decay time scales are most similar to those of water at short times. However, the Ab decay showed longer time scale dynamics; the water peak shift decays to zero by ~1 ps, while the Ab signal contains 2 and 67 ps components. Both decays appear to have some oscillatory character at short times (<300 fs) whereas there do not seem to be any quantum beats in the other solvents. At long times the Ab 6C8 peak shift decays to zero, indicating the absence of inhomogeneous broadening, and that MPTS binds to the Ab in a single, well-defined complex.

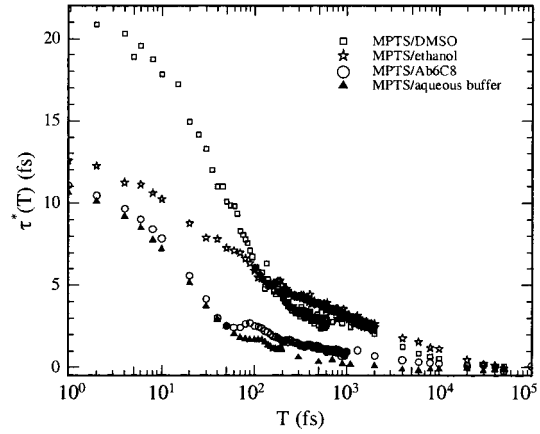

Figure 5. Experimental 3PEPS decays for MPTS in water, DMSO, ethanol, and in Ab6C8.

TABLE 4: Parameters for Direct Exponential Fits of 3PEPS Data

solvent	a_1 (fs)	τ_1 (fs)	a_2 (fs)	τ_2 (fs)	a_3 (fs)	τ_3 (ps)
DMSO	15	40	3.6	150	3.1	4.9
ethanol	6.3	38	2.8	520	2.9	8.7
water	8.7	20	2.1	340		
Ab6C8	9.4	33	1.2	2000	0.6	67

E. MPTS Quantum Chemical Results. For MPTS in both its neutral and deprotonated forms, the CIS results predict the strongly allowed S_1 singlet state to be the lowest excited state, separated by about 0.68 eV from a nearly forbidden S_2 state. (This result contrasts with those for pyrene, where the S_1 state is nearly forbidden and the S_2 state is strongly allowed.[99,93]) The S_0 and S_1 dipole moments were calculated for both the ground and excited state geometries of protonated MPTS. The calculated dipole moments were 2.86 and 3.64 D for S_0 and S_1 in the ground state geometry, and 3.29 and 3.79 D in the excited state geometry. These results predict small changes in the magnitude of the molecular dipole moment ($\Delta\mu$) upon excitation. The calculated structures of the ground and excited state MPTS pyrene core (protonated and deprotonated) are very similar to those reported by Goodpaster et al. for pyrene itself.[93] Both ground and excited state optimized geometries are planar in the core, therefore, only in-plane vibrational modes contribute to the relaxation. The HF and DFT estimates of the MPTS reorganization energy, after scaling of the vibrational frequencies (see Quantum Chemical Methods, above) are 2129 and 1884 cm^{-1}, respectively. Table 5 details the vibrations that are predicted to be the major components of the reorganization. The MPTS frequencies and displacements were used to calculate spectral densities from eq 12, assuming a vibrational dephasing time of 2 ps for all modes. The results are shown in Figure 6.

There are three areas of concern with the calculations. Quantum chemical methods are most developed for the prediction of ground state, not excited state properties. As a result, the largest errors are expected in the excited state geometry and will result in errors in the calculated displacements. Our observation that the reorganization energies are too large, despite scaling of the frequencies, is consistent with this reasoning. Despite such errors, the ground state frequency calculations are likely to be sufficiently accurate to simulate absorption spectra due to the observed solvent broadening.

A second concern regarding the quantum chemistry calculations is the neglect of solvation. It is clear from the solvent dependence of MPTS absorption line shape that the chromophore vibronic structure changes with solvent, especially in the region of ω~1000 cm^{-1}. Raman studies of many chro-

TABLE 5: Frequencies, Displacements, and Reorganization Energies of the 20 Most Strongly Displaced Modes from DFT/CIS Calculation of Protonated MPTS[a]

ω (cm^{-1})	Δ	λ (cm^{-1})
218	−0.51466	28.9
248	0.29834	11.0
447	−0.46059	47.4
1165	0.16909	16.6
1182	−0.34222	69.2
1217	0.31551	60.6
1220	0.18541	21.0
1236	−0.17740	19.5
1242	0.24825	38.3
1246	−0.22492	31.5
1261	−0.27252	46.8
1313	0.75896	378.2
1365	0.19677	26.4
1371	−0.13368	12.2
1398	−0.69224	335.0
1400	0.22673	36.0
1432	0.16266	18.9
1560	−0.23213	42.0
1610	−0.12084	11.8
1677	0.80291	540.4

[a] These modes account for more than 95% of λ_{MPTS}.

mophores, especially charge transfer complexes, demonstrate that vibrational frequencies and displacements may be solvent dependent.[89,101] This solvent dependence is not always apparent in broad, featureless absorption spectra but is clear in MPTS due to its highly structured spectra.

A final concern regarding any calculations based on the Born−Oppenheimer approximation is the neglect of non-Franck−Condon vibrational effects, such as vibronic mixing of S_1 and S_2 electronic states.[102] These effects may be responsible for the missing intensity at $\omega > 2000$ cm^{-1}, a region in which the only fundamental vibrations are C−H modes, which do not typically show significant Franck−Condon activity. The intensity of the combination or overtone bands may result from the proximity of the S_2 state, which lies at 34 500 cm^{-1}.

Despite the difficulties of accurately predicting the MPTS vibrational structure, all calculations consistently demonstrate the relatively small contribution of low frequency (<1000 cm^{-1}) vibrations to $\rho_{MPTS}(\omega)$. This conclusion is independent of theoretical method (HF or DFT) as well as protonation state of the sulfonate groups. The dominant contribution to the spectral width at low frequency is therefore environmental. An accurate fit to the low frequency portion of the absorption spectra and 3PEPS decays requires accurate modeling of environmental dynamics as opposed to a precise knowledge of the MPTS vibrational structure. The success of the model described below, which employs the calculated spectral densities, implies that for cases where Raman spectra are not experimentally available, calculations provide a reasonable alternative for simulating condensed phase spectra.

F. Modeling of 3PEPS Data. A model spectral density must be constructed that reproduces both the 3PEPS signal and the absorption spectra within the constraint of the total reorganization energy. The total reorganization energy and spectral density are approximated as the sum of two components: $\lambda_{total} = \lambda_E + \lambda_{MPTS}$ and $\rho_{total}(\omega) = \rho_E(\omega) + \rho_{MPTS}(\omega)$, where the subscript E refers to either the solvent or Ab environment. (Throughout this manuscript λ_E and $\rho_E(\omega)$ are used to refer to either the solvent or Ab environment, λ_{Ab} and $\rho_{Ab}(\omega)$ are used in cases referring specifically to the Ab environment). This partitioning implies an environment-independent λ_{MPTS} and $\rho_{MPTS}(\omega)$, as is commonly assumed. We therefore sought a single MPTS spectral density that, along with a variable environmental spectral density, allowed for the reproduction of all the 3PEPS decays and absorption spectra.

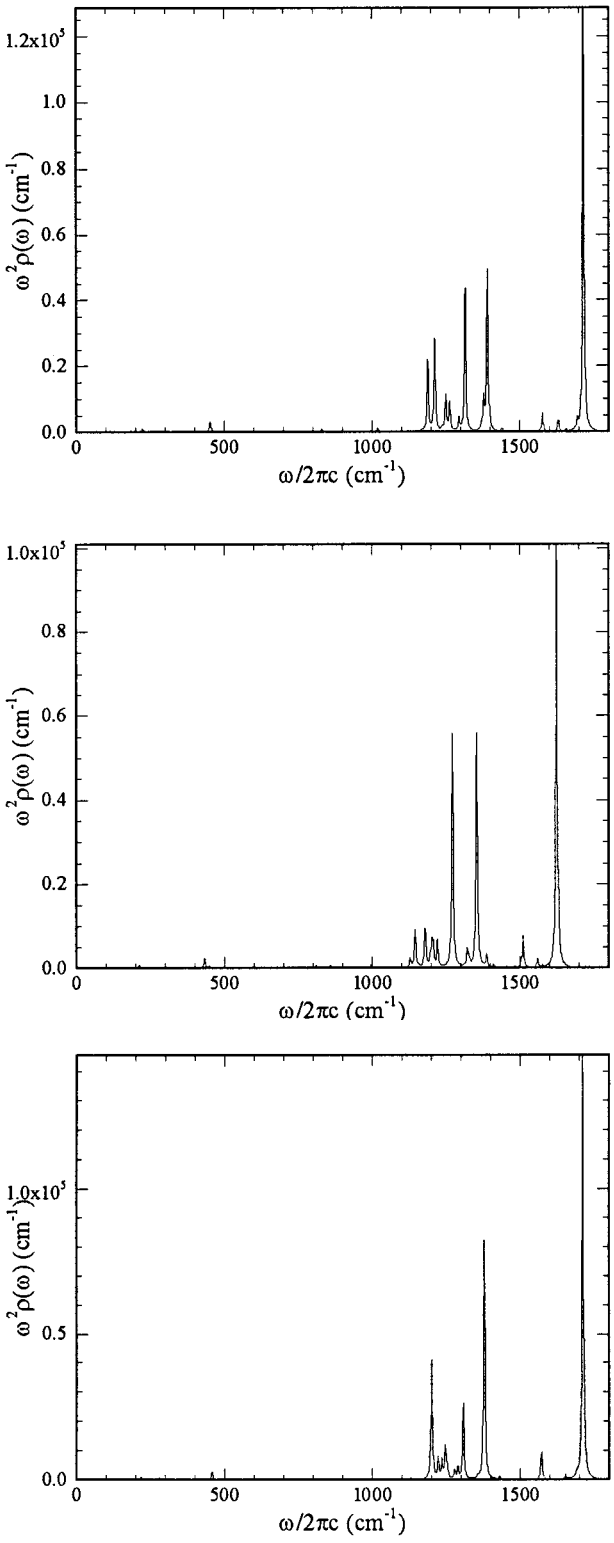

Figure 6. The coupling strength weighted spectral density for MPTS vibrations, $\omega^2\rho_{MPTS}(\omega)$ for MPTSH by HF/CIS (top), and DFT/CIS (center) methods and $MPTS^{3-}$ with the HF/CIS method (bottom).

The frequency and amplitude of each mode that contributes to $\rho_{MPTS}(\omega)$ and $\rho_E(\omega)$ were first independently determined and then combined into a total spectral density which was used to simulate the 3PEPS decay and absorption spectra. Finally, adjustments were made to the solvent spectral density in order

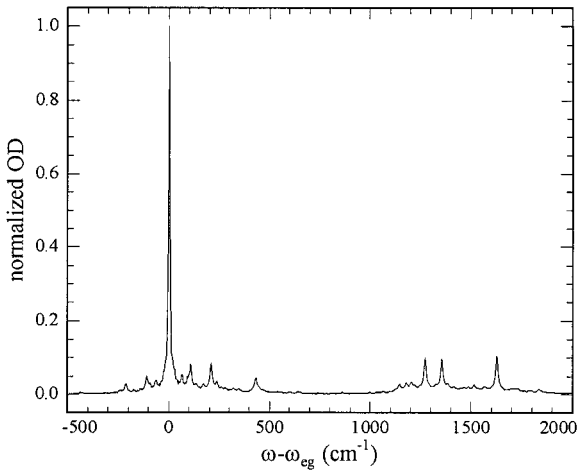

Figure 7. Simulated MPTS spectrum calculated from a DFT/CIS-derived spectral density without solvent broadening.

to improve the fits. HF and DFT calculations show that only a small portion (<10%) of the λ_{MPTS} results from low frequency vibrations (ω < 1000 cm^{-1}) of the chromophore. Specifically, the HF calculations show only two significantly displaced low frequency modes (at 240 and 486 cm^{-1}) with $\lambda\sim$100 cm^{-1}. In the DFT calculations, these same modes appear at 218 and 447 cm^{-1} with $\lambda\sim$80 cm^{-1}. This vibronic structure implies that the width (σ_{0-0}) and shift ($\omega_{eg}-\omega_{abs}$) of the low frequency region of the spectrum are primarily determined by the solvent spectral density rather than by vibrational structure (Figure 7). Therefore, the initial model $\rho_E(\omega)$ was generated by fitting the low frequency portion of the absorption spectrum. The number of components used to construct the solvent spectral density followed from the number of decay components used to fit the 3PEPS decays. For example, MPTS/DMSO 3PEPS showed two exponential components, with 160 fs and 4.9 ps time scales; therefore, two decay components were included in $\rho_E(\omega)$, with frequencies corresponding to the inverse of these time scales. Both Lorentzian and Gaussian functions were used to fit the data. The relative amplitudes were determined from the exponential fits to the 3PEPS data, and λ_E was varied in order to reproduce the low frequency (ω < 1000 cm^{-1}) region of the spectra.

The term $\rho_{MPTS}(\omega)$ was determined with the quantum chemistry methods described above. Although it is more reasonable that a small number of modes change their displacements and/or frequencies due to solvation, we chose to scale the entire $\rho_{MPTS}(\omega)$, as the scaling of individual modes is arbitrary without appropriate data. To compensate for the overestimated value for λ_{MPTS} a constant amplitude scaling factor was sought that would give a $\rho_{MPTS}(\omega)$ suitable for the simulation of all the data. We found that the value of λ_{MPTS} determines the ratio of the lowest energy "0-0" peak to that of the next higher energy vibronic band. A value of $\sim$1000 cm^{-1} is most consistent with the entire set of data (Ab and 3 solvents). Increasing the contribution of λ_{MPTS} decreases the initial peak shift and increases the amplitude of oscillatory components in the 3PEPS decay.

Equation 9 was used to simulate the 3PEPS experiment. Simulations were performed with pulse widths ranging from 35 to 50 fs fwhm, and only minor effects were apparent in the calculated peak shifts. The pulse width does affect the amplitude of the oscillatory components; however, these oscillations, due to impulsively excited intramolecular modes at 218 and 447 cm^{-1}, are not an important focus of the present inquiry. We have also simulated the wavelength dependence of the modeled 3PEPS signal, for $|\omega-\omega_{eg}|$ < 400 cm^{-1}, to verify that the time scales and amplitudes are not sensitive to excitation wavelength. The detuning effects are found to be small, due to the low density of strongly coupled vibrations in the low frequency region of the MPTS spectral density.

The 3PEPS data, absorption spectra, and simulations are shown in Figure 8. The environmental spectral densities are shown in Figure 9. Values of λ_{MPTS}, λ_E, and time constants are given in Table 6. The simulations accurately reproduce the time scales and relative amplitudes of the various phases of the 3PEPS decay. The initial values of the peak shifts are overestimated, as is generally observed in other 3PEPS studies in which modeling based on a spectral density or solvent correlation function has been performed. Several explanations have been discussed for this problem, such as an underestimate of the magnitude of the intramolecular contributions,[103,104] detuning, pulse chirp effects, and interference between solvent birefringence and the echo signal.[105] The 400 nm excitation pulses were not characterized by frequency resolved optical gating, or by other methods, to determine the shape of the electric field envelope and the wavelength-dependent phase.[106] Therefore, pulse chirp is the most likely explanation for the remaining discrepancy between the simulations and data.

Absorption spectra were simulated with eq 8. Agreement between simulated and measured absorption spectra is good in the low frequency (<1000 cm^{-1}) region, reasonable in the intermediate frequency (1000−2000 cm^{-1}), but rather poor on the high energy side of the spectra (> 2000 cm^{-1}). The primary source of the discrepancy between measured and simulated absorption spectra most likely results from inaccuracies in the calculated vibrational structure of MPTS, as discussed above. The model spectral densities capture 61% to 73% of the total reorganization energies of MPTS in solvents and MPTS-Ab complexes. Since the discrepancies between the simulated and measured spectra are most pronounced at high frequencies, it is most likely that the magnitude of λ_{MPTS} is underestimated, and the true value of λ_{MPTS} is likely to be between 1478 and 1774 cm^{-1}. Despite the inability of the model to capture the highest frequency vibrational dynamics, the low energy portion of the spectrum, including solvent or protein dynamics, is accurately modeled, and the model gives a good estimate of λ_E and the associated vibrational time scales.

V. Discussion

A. 3PEPS Spectroscopy and Protein Dynamics. Most previous 3PEPS protein studies have focused on photosynthetic proteins, such as bacterial LH1/LH2 complexes and reaction centers,[73,82,84] the B820 subunit of LH1,[83] higher plant LHCII,[85] and allophycocyanin/α-phycocyanin.[107] These experiments have resulted in a detailed understanding of light harvesting; however, the effects of excitation transfer on the 3PEPS signals complicate the measurement of protein fluctuation time scales. In these proteins, the electron−phonon coupling is very weak and the 3PEPS decays exhibit large amplitude ∼100 fs components similar to those of chromophores in solvent, followed by slower components unique to the protein environment. These slower components are usually associated with the excitation transfer process. However, studies of α-phycocyanin (a subunit of allophycocyanin that does not undergo excitation transfer) did show 100 fs and 5.5 ps components that were assigned to protein dynamics.[107] The only nonphotosynthetic complex studied with 3PEPS thus far has been an eosin−lysozyme complex.[60] In this complex, most of the response (80%) was the same as that of aqueous eosin. Two processes, with 7 and 135 ps time scales, were unique to the protein environment. However, these time

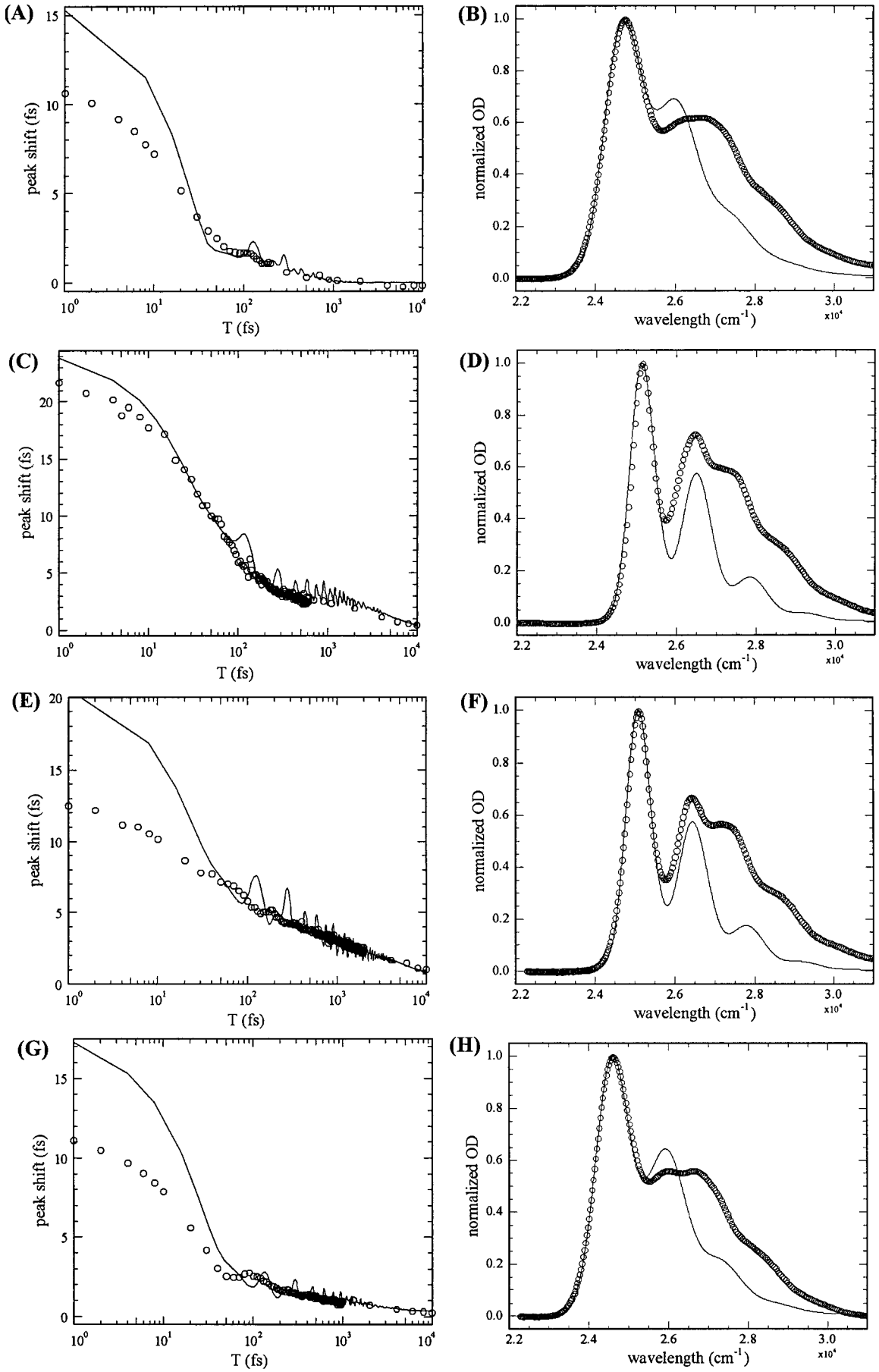

Figure 8. (A) MPTS/water 3PEPS data and fit and (B) absorption spectrum and fit; (C) MPTS/DMSO 3PEPS data and fit and (D) adsorption spectrum and fit; (E) MPTS/ethanol 3PEPS data and fit and (F) absorption spectrum and fit; (G) MPTS/Ab6C8 3PEPS data and fit and (H) absorption spectrum and fit.

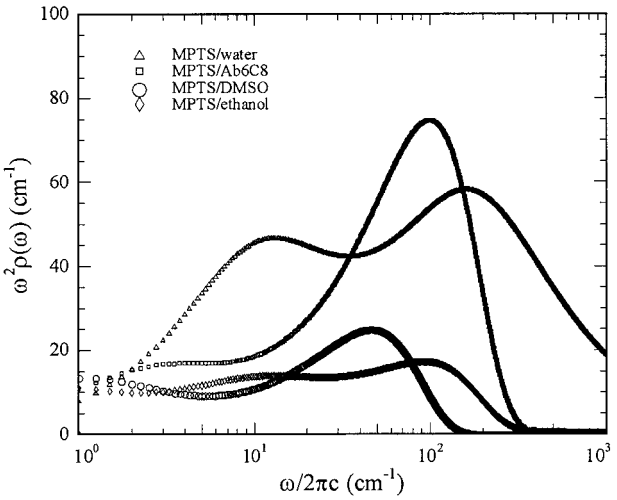

Figure 9. Model solvent spectral densities, $\omega^2\rho_E(\omega)$ used for the simulated 3PEPS decays and absorption spectra in Figure 7. Parameters for constructing these $\rho_E(\omega)$ are given in Table 6.

TABLE 6: Parameters for $\rho_E(\omega)$

solvent	λ_g (cm^{-1})	τ_g (fs)	λ_{e1} (cm^{-1})	τ_{e1} (fs)	λ_{e2} (cm^{-1})	τ_{e2} (fs)	λ_{e3} (cm^{-1})	τ_{e3} (ps)
DMSO	102	160	81	5000				
water			335	30	250	500		
ethanol	62	75	63	520	63	8700		
Ab6C8			306	75	80	2000	46	67

scales are similar to those observed in frequency-dependent dielectric measurements on hydrated lysozyme powders (4 and 270 ps) that measure protein associated water relaxation.[108] The important role of solvent likely results from eosin binding to a "hydrophobic box" of the protein, an interaction that is nonspecific, low affinity (3 μM), and not likely to shield eosin from the aqueous environment.

In contrast, the immunologically generated Ab show high affinity (nM) and specificity for MPTS. The interactions between the protein and the chromophore are expected to be typical of those commonly employed within any Ab−Ag complex, or more generally, between any protein and ligand, cofactor, or substrate. The current study reports the reorganization energies for a family of anti-MPTS Ab, as well as the 3PEPS study of one complex, Ab 6C8-MPTS. The reorganization energies and the associated time scales allow for the characterization of these complexes in terms of protein flexibility. Before the dynamics of Ab 6C8 are described, a discussion of the MPTS probe is first presented.

B. MPTS as a Probe of Solvation and Protein Dynamics. In the simplest description, solvent polarity has an effect on absorption and emission frequencies that is due to the differential stabilization (solvation) of the chromophore ground and excited electronic state dipoles by the solvent dipoles.[58] This simple dipolar interaction model predicts that when the dipole moment of the excited state is larger than that of the ground state, the absorption spectrum will shift to lower frequencies (red shift) with increasing solvent polarity. The opposite effect (blue shift) will be observed if the excited state dipole moment is smaller than the ground state dipole moment. As discussed above, solvent studies show that the excited state of MPTS is more polar than the ground state.

Although quantum chemistry calculations predict that MPTS undergoes only a 0.8 D change in dipole moment upon excitation, steady state measurements on MPTS show that it is quite sensitive to solvent polarity. Based on a comparison to coumarin 153 (which undergoes an approximately 8 D change upon excitation and shows up to 2400 cm^{-1} solvent reorganization energies), simple dipolar reaction field models, with linear dependency of $\Delta\nu$ on $\Delta\mu$, predict that MPTS solvent reorganization energies should be on the order of 200 cm^{-1}. The observed environmental reorganization energies, λ_E, are consistent with this model, ranging between 180 and 585 cm^{-1}.

The origin of the solvent sensitivity may be understood by comparing MPTS to PTS and HPTS. PTS is a symmetric molecule and therefore has no permanent dipole moment in either S_0 or S_1, so dipolar solvation effects should be negligible. In agreement with this prediction, λ_{PTS} changes by only 70 cm^{-1} for the solvents studied. HPTS, with an 8-OH group, should not be significantly more dipolar than MPTS. However, HPTS show larger changes in the reorganization energy and absorption line shape due to the solvent environment. Furthermore, Pines and co-workers have shown that the peak-to-valley ratio in the absorption spectrum of HPTS is linearly correlated with the fluorescence maximum, which was shown to be linearly correlated with solvent polarity based on a number of empirical polarity scales.[109] Clearly, the symmetry-lowering effect of substituents on the pyrene ring not only introduces a permanent dipole moment but also changes the selection rules for the vibrational transitions and the frequencies and displacements of the Franck−Condon active modes. The hypothesis that the MPTS S_0-S_1 energy gap fluctuates due to polar interactions with the solvent is supported by our observation that the time scales of MPTS solvation are similar to those of dipolar probe-molecule solvation observed in other studies.

The MPTS solvation time scales in water, DMSO, and ethanol may be compared to those from other 3PEPS measurements or time scales of the solvent response functions derived from time-resolved fluorescence Stokes shift measurements (TRFSS).[95] Both types of experiments utilize solvation probes that have large dipole moments and large $\Delta\mu$. We focus on components of time scales longer than 100 fs, since in both types of experiment, these are the time scales most accurately determined and ascribed to solvation dynamics. Time scales from each solvent are discussed below.

Aqueous solvation of coumarin 343 in water was studied by Jimenez et al., who employed TRFSS to characterize solvation response time scales of 55, 126, and 880 fs.[110] Lang et al. used 3PEPS measurements to characterize 17 fs, 400 fs, and 2.7 ps solvation times for aqueous eosin.[77] (The origin of the 2.7 ps component in the eosin measurements was not fully explained, but it may result from the dynamics of eosin−water hydrogen-bonding interactions.) The MPTS 3PEPS data in water show time scales of 20 and 337 fs. All three experiments demonstrate that more than 70% of the decay occurs on the sub-50 fs time scale. Each experiment also observed a smaller amplitude (~20%) subpicosecond component of the solvation. However, the solvation dynamics of MPTS does not include the long ps time scale water motion apparent with solvation of coumarin 343 or eosin.

Solvation dynamics measurements on coumarin 153 in DMSO with TRFSS found 200 fs, 2.3 ps, and 10.7 ps time scales.[95] In their 3PEPS experiments on rhodamine 6G in DMSO, Xu et al. observed 100 fs, 2.3 ps, and 62 ps time scales.[97] The MPTS/DMSO time scales of 146 fs and 4.9 ps are qualitatively in agreement with the other two results, except for the 62 ps component from the rhodamine 6G measurements. As with water solvation, DMSO solvation of MPTS does not show the longest time scale dynamics observed with the other solvatochromic probes.

For ethanol solvation dynamics, TRFSS measurements with coumarin 153 revealed 390 fs, 5 ps, and 30 ps time constants, whereas 3PEPS experiments with rhodamine showed time scales of 250 fs, 3.4 ps, and 28 ps. MPTS solvation dynamics in ethanol show time scales of 520 fs and 8.7 ps. The results all agree qualitatively in showing a subpicosecond component followed by a 5−10 ps component. However, MPTS does not show the ∼30 ps time scale revealed by the other two measurements.

Agreement between the MPTS solvation time scales from the current investigation with those from previous measurements show that the MPTS 3PEPS measurements follow the time scales of the molecular motions of these liquids. Our results, especially for the faster dynamics, with MPTS in water, DMSO, and ethanol show solvation dynamics time scales that are commensurate with those of other commonly employed solvatochromic probes. The exception is the absence of the longest time scale solvation dynamics when probed with MPTS. This might result from specific (hydrogen-bonding) interactions between the solvent and probe molecule; coumarin 343, eosin, and rhodamine 6G each have strong hydrogen-bond accepting groups, while rhodamine 6G also has two hydrogen-bond amines and MPTS has neither. The potentially slower dynamics of tightly bound solvent is consistent with the observation that rhodamine 6G, the only probe with a hydrogen-bond donor group, shows the longest time-scale dynamics in DMSO, which is a hydrogen-bond acceptor but not a donor. The inability of MPTS to participate in strong hydrogen-bonding interactions with the solvent might explain the consistent absence of the slow time scale solvation dynamics for this probe.

C. Antibody Dynamics. MPTS is tightly bound by the Ab. Upon excitation of MPTS, an instantaneous force is applied to the Ab due to the charge redistribution in the chromophoric Ag. The subsequent relaxation processes result in chromophore fluorescence at a longer wavelength (lower energy) than absorption. The energetics and dynamics of this reorganization process may be experimentally determined. Before the detailed analysis of the Ab 6C8-MPTS complex is discussed, it is interesting to examine the magnitude and trends of the total reorganization energy of the MPTS−Ab complexes. Based on simulation of the Ab 6C8 absorption spectra with various λ_{MPTS}, it was determined that the value of λ_{MPTS} was correlated with the intensity ratio between the lowest energy peak in the absorption spectrum and the first vibronic sideband. This ratio is roughly constant in each Ab (see Figure 3). Therefore, λ_{MPTS} is likely to be approximately constant in each environment. From the full analysis described above, λ_{MPTS} is approximately 1500 cm^{-1} when bound to Ab 6C8. Therefore, the λ_{Ab} range between 50 and 500 cm^{-1}. The wide distribution of reorganization energies implies that the immune system is capable of generating a wide variety of dynamic combining sites that can bind MPTS. Moreover, the magnitude of the observed protein energetics is remarkable. In fact, the energy of these protein motions approaches 15% of the average binding free energy (∼3400 cm^{-1}).

Although λ_{Ab} contains information about fluctuation energetics, an interpretation based on protein dynamics requires additional data. λ_{Ab} is the product of the frequencies and the squared displacements of the vibrations; therefore, the time scales of the vibrations must be determined independently. For example, an Ab with low frequency vibrations (small force constants) will be capable of greater displacements for a fixed energy, while one with higher frequency motions (large force constants) will require larger amounts of energy for the same displacements. The former Ab is more flexible than the latter. To accurately determine λ_{Ab}, and the associated conformational flexibility, the spectral density of the fluctuations was determined by fitting the 3PEPS data.

The time scales of the motions induced upon chromophore excitation are available from the spectral density, $\rho_{Ab}(\omega)$. Three specific protein motions are observed in the Ab 6C8-MPTS complex upon charge redistribution of the chromophore. A large amplitude, ultrafast protein motion was observed, accounting for 71% of the protein reorganization energy on a 75 fs time scale (corresponding to 445 cm^{-1}). Slower Ab dynamics were also observed. Protein vibrations with time scales of 2 and 67.4 ps (corresponding to 16.7 and 0.5 cm^{-1}, respectively) accounted for 18% and 11%, of the combining site reorganization energy, respectively.

To discuss protein motions that might give rise to the observed dynamics, it is useful to first describe several structural aspects of the Ab combining site that are conserved in virtually all Ab−Ag complexes.[39] Ab result from the heterodimerization of light and heavy polypeptide chains. Six "complementarity determining regions", three from the light chain (LC CDR 1−3) and three from the heavy chain (HC CDR 1−3), comprise a roughly C_2 symmetric combining site. The CDR3 loops from each chain form the center of the combining site and are typically the major components of a deep binding cleft for small molecule Ag. These binding clefts are typically hydrophobic, tightly pack the Ag, and exclude water. It is therefore likely that MPTS is tightly packed by the Ab CDR3 loops, rendering it electrostatically coupled to protein motions but shielded from water.

A variety of protein motions are consistent with both the observed time scales and Ab combining site structures. The ultrafast response may be inertial and may result from nearly free motion of a polar side chain within a CDR3 loop. However, most polar side chains are expected to be engaged in strong hydrogen-bond or salt-bridge interactions and are therefore unlikely to be involved in an inertial response. However, methionine and phenylalanine are each relatively noninteracting and polar. For example, benzene and other "nondipolar" solvents have been shown to cause ultrafast inertial solvation of coumarin.[96] Therefore, the large amplitude 75 fs response in Ab 6C8 may correspond to motion of a CDR3 loop methionine or phenylalanine side chain. In the HC and LC CDR3 loops, 6C8 has a single phenylalanine residue (Phe100 in the heavy chain) and no methionine residues. It is possible, therefore, that motion of Phe100 contributes to the 6C8 combining site reorganization. Interestingly, structural studies have implicated that aromatic residues at similar positions of the HC CDR3 undergo significant reorganization upon ligand binding in other Ab.[53] Alternatively, if sufficiently coupled, lower amplitude, collective motion of less mobile side chains, such as those from hydrogen-bonded aspartic acid or arginine, may be the origin of the ultrafast response.

The picosecond dynamics are likely to result from CDR3 amino acid side chain librations as well as entire loop motions, if the loop is sufficiently flexible. For example, based on NMR relaxation studies, it has been speculated that each light chain residue of anti-digoxin Ab 26−10 undergoes ps-time scale motion corresponding to barrier-free librations of amide groups.[45] Both 6C8 light and heavy chain CDR3 loops contain aromatic and charged residues. However, the flexibility of the two loops is expected to be distinctly different. The LC CDR3 is 8 residues long and contains no glycine residues, while the HC CDR3 is 14 residues long and contains 4 glycine residues, of which two

are consecutive. The HC CDR3 is expected to be highly flexible. Therefore, motion of charged residues contained in the flexible HC CDR3 loops may be the origin of the ps time scale motions in Ab 6C8.

The molecular origins of both the ultrafast and ps time scale motions within the combining site of 6C8 are at present only speculative. However, structural studies are currently underway. Structural data will be used, along with dynamics simulations, to more quantitatively assign the structural basis of the protein motions.

Conclusions

Conformational dynamics may play an important role in Ab−Ag recognition and in protein function in general. For example, the lock-and-key and induced fit mechanisms of Ag recognition are differentiated by the conformational flexibility of the Ab combining site. In the lock-and-key model, an Ab combining site has a rigid, fixed shape and charge distribution that is complementary to a given Ag shape and charge. This combining site configuration represents a well-defined structure, i.e., a global minimum on the potential energy surface that is well separated from other regions of the surface by relatively high energy barriers. With bound Ag, such Ab are expected to resist structural distortions by responding to an applied force with high frequency motions. In contrast, the induced fit model posits that an Ab combining site is not strongly localized to a single structure, but rather is only a local minimum on the energy surface that is separated from other local minima by relatively low energy barriers. These Ab, when bound to Ag, are expected to succumb to structural distortions by responding to an applied force with low frequency motions. The combining site is therefore able to interconvert among the possible local minima, which correspond to unique combining site structures. To understand this dynamic behavior, the energetics and time scales of the protein motions must be individually determined. For the Ab 6C8-MPTS complex, charge redistribution in the Ag induces three protein motions, the first, with $\lambda_{Ab1} = 306$ cm^{-1} and $\tau_{Ab1} = 75$ fs, the second, with $\lambda_{Ab2} = 80$ cm^{-1} and $\tau_{Ab2} = 2$ ps, and the third, with $\lambda_{Ab3} = 67$ cm^{-1} and $\tau_{Ab3} = 67$ ps. These motions are superpositions of vibrations that are likely to be associated with CDR3 loop or side chain motions in the Ab combining site. This frequency and amplitude response for a given Ab are conveniently given as $\rho_{Ab}(\omega)$, which is therefore the most useful characterization of the protein in terms of conformational flexibility. Comparison of the $\rho_{Ab}(\omega)$ of different Ab−Ag complexes will serve as a basis for quantitating the relative flexibilities of the proteins.

A full understanding of the protein dynamics of the Ab6C8−MPTS complex requires determination of the force constants. This requires a molecular interpretation of the motion to determine the associated reduced masses. Crystallographic, molecular dynamics, and mutagenesis studies are currently in progress toward this end. Having established a protocol to quantitate the conformational flexibility of Ab−Ag complexes, we are in the process of analyzing multiple complexes between MPTS and other anti-MPTS Ab isolated during the immune response. This analysis should allow for a quantitation of the relative roles of lock-and-key and induced fit mechanism of Ag recognition.

Acknowledgment. Funding provided by the Skaggs Institute for Chemical Biology and the National Institutes of Health (GM 56879, D.A.C). We thank Prof. Taiha Joo for helpful discussions.

Supporting Information Available: Results of quantum chemical calculations on MPTS. This material is available free of charge via the Internet at http://pubs.acs.org.

References and Notes

(1) Frauenfelder, H.; Sligar, S. G.; Wolynes, P. G. *Science* **1991**, *254*, 1598.
(2) Karplus, M.; McCammon, J. A. *Annu. Rev. Biochem.* **1983**, *53*, 263.
(3) Welch, G. R. *The Fluctuating Enzyme*; Wiley-Interscience: New York, 1986; Vol. V.
(4) Chan, H. S.; Dill, K. A. *Proteins Struct. Funct. Genet.* **1998**, *30*, 2.
(5) *Mechanisms of Protein Folding*; Pain, R. H., Ed.; IRL Press: Oxford, 1994; Vol. 3.
(6) *Special Issue on Protein Folding*; Winkler, J. R., Gray, H. B., Eds.; *Acc. Chem. Res.* **1998**, *31*, 697−780.
(7) Radford, S. E. *Trends Biochem. Sci.* **2000**, *25*, 611.
(8) Koshland, D.; Nemethy, G.; Filmer, D. *Biochemistry* **1966**, *5*, 364.
(9) Akke, M.; Forsén, S.; Chazin, W. J. *J. Mol. Biol.* **1991**, *220*, 173.
(10) Monod, J.; Wyman, J.; Changeux, J.-P. *J. Mol. Biol.* **1965**, *12*, 88.
(11) Lumry, R.; Gregory, R. B. Free-energy management in protein reactions: concepts, complications, and compensation. In *The Fluctuating Enzyme*; Welch, G. R., Ed.; Wiley-Interscience: New York, 1986; p 1.
(12) Lumry, R.; Gregory, R. B. *J. Mol. Liq.* **1989**, *42*, 133.
(13) Huang, K.; Ghose, R.; Flanagan, J. M.; Prestegard, J. H. *Biochemistry* **1999**, *38*, 10567.
(14) Binda, C.; Angelini, R.; Federico, R.; Ascenzi, P.; Mattevi, A. *Biochemistry* **2001**, *40*, 2766.
(15) Paulsen, M. D.; Ornstein, R. L. *Proteins Struct. Funct. Genet.* **1995**, *21*, 237.
(16) Berzofsky, J. A. *Science* **1985**, *229*, 932.
(17) Bostock-Smith, C. E.; Harris, S. A.; Laughton, C. A.; Searle, M. S. *Nucleic Acids Res.* **2001**, *29*, 693.
(18) Martin, J. R.; Mulder, F. A. A.; Karimi-Nejad, Y.; van der Zwan, J.; Mariani, M.; Schipper, D.; Boelens, R. *Structure* **1997**, *5*, 521.
(19) Gerstein, M.; Lesk, A. M.; Chothia, C. *Biochemistry* **1994**, *33*, 6739.
(20) Patten, P. A.; Gray, N. S.; Yang, P. L.; Marks, C. B.; Wedemayer, G. J.; Boniface, J. J.; Stevens, R. C.; Schultz, P. G. *Science* **1996**, *271*, 1086.
(21) Wedemayer, G. J.; Patten, P. A.; Wang, L. H.; Schultz, P. G.; Stevens, R. C. *Science* **1997**, *276*, 1665.
(22) Deng, H.; Zhadin, N.; Callender, R. *Biochemistry* **2001**, *40*, 3767.
(23) McCammon, J. A. *Curr. Opin. Struct. Biol.* **1998**, *8*, 245.
(24) Zhou, H.-X.; Wlodek, S. T.; McCammon, J. A. *Proc. Natl. Acad. Sci. U.S.A.* **1998**, *95*, 9280.
(25) Varley, P. G.; Pain, R. H. *J. Mol. Biol.* **1991**, *220*, 531.
(26) Wrba, A.; Schweiger, A.; Schultes, V.; Jaenicke, R.; Závodszky, P. *Biochemistry* **1990**, *29*, 7584.
(27) Huber, R. *Trends Biochem. Sci.* **1979**, *4*, 271.
(28) Schmidt, R. K.; Gready, J. E. *J. Mol. Model.* **1999**, *5*, 153.
(29) Farnum, M. F.; Madge, D.; Howell, E. E.; Hirai, J. T.; Warren, M. S.; Grimsley, J. K.; Kraut, J. *Biochemistry* **1991**, *30*, 11567.
(30) Careri, G.; Gratton, E. The statistical time correlation approach to enzyme action: The role of hydration. In *The Fluctuating Enzyme*; Welch, G. R., Ed.; Wiley-Interscience: New York, 1986; p 227.
(31) Gavish, B. Molecular dynamics and the transient strain model of enzyme catalysis. In *The Fluctuating Enzyme*; Welch, G. R., Ed.; Wiley-Interscience: New York, 1986; p 263.
(32) Somogyi, B.; Damjanovich, S. A. A microenvironmental approach to enzyme dynamics. In *The Fluctuating Enzyme*; Welch, G. R., Ed.; Wiley-Interscience: New York, 1986; p 341.
(33) Kraut, J. *Science* **1988**, *242*, 533.
(34) Lumry, R. Mechanical force, hydration, and conformational fluctuations in enzymic catalysis. In *A Study of Enzymes*; Kuby, S. A., Ed.; CRC Press: Boca Raton, FL, 1991; Vol. II.
(35) Kuznetsov, A. M. *Charge Transfer in Physics, Chemistry, and Biology: Physical Mechanisms of Elementary Processes and an Introduction to the Theory*; Gordon & Breach: Amsterdam, New York, 1995.
(36) Bendall, D. S. *Protein Electron Transfer*; Bios Scientific: Oxford, 1996.
(37) Flynn, P. F.; Urbauer, R. J. B.; Zhang, H.; Lee, A. L.; Wand, A. J. *Biochemistry* **2001**, *40*, 6559.
(38) Pochapsky, T. C.; Kostic, M.; Jain, N.; Pejchal, R. *Biochemistry* **2001**, *40*, 5602.
(39) Nezlin, R. *The Immunoglobulins: Structure and Function*; Academic Press: New York, 1998.
(40) Kuby, J. *Immunology*, 2nd ed; W. H. Freeman and Company: New York, 1994.
(41) *Somatic Hypermutation in V−Regions*; Steele, E. J., Ed.; CRC Press: Boca Raton, FL, 1990.

(42) Koshland, D. E.; Neat, K. E. *Annu. Rev. Biochem.* **1968**, *37*, 359.
(43) Pauling, L. *Chem. Eng. News* **1946**, *24*, 1375.
(44) Haldane, J. B. S. *Enzymes*; Green and Bo: London, 1930.
(45) Constantine, K. L.; Friedrichs, M. S.; Goldfarb, V.; Jeffrey, P. D.; Sheriff, S.; Mueller, L. *Proteins Struct. Funct. Genet.* **1993**, *15*, 290.
(46) Constantine, K. L.; Goldfarb, V.; Wittekind, M.; Anthony, J.; Ng, S.-C.; Mueller, L. *Biochemistry* **1992**, *31*, 5033.
(47) Lim, K.; Herron, J. N. *Biochemistry* **1995**, *34*, 6962.
(48) Stella, L.; Nicotra, M.; Ricci, G.; Rosata, N.; Di Ioria, E. E. *Proteins Struct. Funct. Genet.* **1999**, *37*, 1.
(49) Buchberger, A.; Howard, M. J.; Freund, S. M. V.; Proctor, M.; Butler, P. J. G.; Fersht, A. R.; Bycroft, M. *Biochemistry* **2000**, *39*, 11137.
(50) Peters, G. H.; Bywater, R. P. *Prot. Engineer.* **1999**, *12*, 747.
(51) Karslake, C.; Botuyan, M. V.; Gorenstein, D. G. *Biochemistry* **1992**, *31*, 1849.
(52) Carr, P. A.; Erickson, H. P.; Palmer, A. G. I. *Structure* **1997**, *5*, 949.
(53) Rini, J. M.; Schulze-Gahmen, U.; Wilson, I. A. *Science* **1992**, *255*, 959.
(54) Williams, R. J. P. *Eur. Biophys. J.* **1993**, *21*, 393.
(55) Jardetzky, O.; Lefèvre, J. F. *FEBS Lett.* **1994**, *338*, 246.
(56) Ishima, R.; Torchia, D. A. *Nat. Struct. Biol.* **2000**, *7*, 740.
(57) Harlow, E.; Lane, D. *Antibodies: a Laboratory Manual*; Cold Spring Harbor Laboratory: Cold Spring Harbor, 1988.
(58) Reichardt, C. *Solvents and Solvent Effects in Organic Chemistry*, 2nd ed; VCH Verlagsgesellschaft mbH: Weinheim, 1990.
(59) Fleming, G. R.; Cho, M. *Annu. Rev. Phys. Chem.* **1996**, *47*, 109.
(60) Jordanides, X. J.; Lang, M. J.; Song, X.; Fleming, G. R. *J. Phys. Chem. B* **1999**, *103*, 7995.
(61) Lim, M.; Hamm, P.; Hochstrasser, R. M. *Proc. Natl. Acad. Sci. U.S.A.* **1998**, *95*, 15315.
(62) de Boeij, W. P.; Pshenichnikov, M. S.; Wiersma, D. A. *Annu. Rev. Phys. Chem.* **1998**, *49*, 99.
(63) Bardeen, C. J.; Rosenthal, S. J.; Shank, C. V. *J. Phys. Chem. A* **1999**, *103*, 10506.
(64) Yang, T. S.; Chang, M. S.; Chang, R.; Hayashi, M.; Lin, S. H.; Vohringer, P.; Dietz, W.; Scherer, N. F. *J. Chem. Phys.* **1999**, *110*, 12070.
(65) Mukamel, S. *Principles of Nonlinear Optical Spectroscopy*; Oxford University Press: New York, 1995.
(66) de Boeij, W. P.; Pshenichnikov, M. S.; Duppen, K.; Wiersma, D. A. *Chem. Phys. Lett.* **1994**, *224*, 243.
(67) de Boeij, W. P.; Pshenichnikov, M. S.; Wiersma, D. A. *Chem. Phys. Lett.* **1996**, *253*, 53.
(68) de Boeij, W. P.; Pshenichnikov, M. S.; Wiersma, D. A. *J. Phys. Chem.* **1996**, *100*.
(69) Nibbering, E. T. J.; Duppen, K.; Wiersma, D. A. *J. Chem. Phys.* **1990**, *93*, 5477.
(70) Nibbering, E. T. J.; Wiersma, D. A.; Duppen, K. Femtosecond photon echo formation in liquids. In *Coherence Phenomena in Atoms and Molecules in Laser Fields*; Bandrauk, A. D., Wallace, S. C., Eds.; Plenum Press: New York, 1992; p 377.
(71) Book, L. D.; Ostafin, A. E.; Ponomarenko, N.; Norris, J. R.; Scherer, N. F. *J. Phys. Chem. B* **2000**, *105*, 8295.
(72) Arnett, D. C.; Moser, C. C.; Dutton, P. L.; Scherer, N. F. *J. Phys. Chem. B* **1999**, *103*, 2014.
(73) Salverda, J. M.; van Mourik, F.; van der Zwan, G.; van Grondelle., R. *J. Phys. Chem. B* **2000**, *104*, 11395.
(74) Passino, S. A.; Nagasawa, Y.; Joo, T.; Fleming, G. R. *J. Phys. Chem. A* **1997**, *101*, 725.
(75) Larsen, D. S.; Ohta, K.; Fleming, G. R. *J. Chem. Phys.* **1999**, *111*, 8970.
(76) Lee, S.-H.; Lee, J.-H.; Joo, T. *J. Chem. Phys.* **1999**, *110*, 10969.
(77) Lang, M. J.; Jordanides, X. J.; Song, X.; Fleming, G. R. *J. Chem. Phys.* **1999**, *110*, 5884.
(78) Joo, T.; Jia, Y.; Yu, J.-Y.; Lang, M. J.; Fleming, G. R. *J. Chem. Phys.* **1996**, *104*, 6089.
(79) Cho, M.; Yu, J.-Y.; Joo, T.; Nagasawa, Y.; Passino, S. A.; Fleming, G. R. *J. Phys. Chem.* **1996**, *100*, 11944.
(80) Nagasawa, Y.; Passino, S. A.; Joo, T.; Fleming, G. R. *J. Chem. Phys.* **1997**, *106*, 4840.
(81) Nagasawa, Y.; Yu, J.-Y.; Fleming, G. R. *J. Chem. Phys.* **1998**, *109*, 6175.
(82) Groot, M.-L.; Yu, J.-Y.; Agarwal, R.; Norris, J. R.; Fleming, G. R. *J. Phys. Chem. B* **1998**, *102*, 5923.
(83) Yu, J.-Y.; Nagasawa, Y.; van Grondelle, R.; Fleming, G. R. *Chem. Phys. Lett.* **1997**, *280*, 404.
(84) Jimenez, R.; van Mourik, F.; Yu, J. Y.; Fleming, G. R. *J. Phys. Chem. B* **1997**, *101*, 7350.
(85) Agarwal, R.; Kruegger, B. P.; Scholes, G. D.; Yang, M.; Yom, J.; Mets, L.; Fleming, G. R. *J. Phys. Chem. B* **2000**, *104*, 2908.
(86) *Antibody engineering: a practical approach*; McCafferty, J., Hoogenboom, H. R., Chiswell, D. J., Eds.; Oxford University Press: Oxford, 1996; Vol. 169.
(87) Parker, C. A. *Photoluminesence of solutions*; Elsevier: Amsterdam, 1968.
(88) Schomacker, K. T.; Champion, P. M. *J. Chem. Phys.* **1986**, *84*, 5314.
(89) Myers, A. B. *Chem. Rev.* **1996**, *96*, 911.
(90) Wright, P. G.; Stein, P.; Burke, J. M.; Spiro, T. G. *J. Am. Chem. Soc.* **1979**, *101*, 3531.
(91) Mroginski, M.-A.; Németh, K.; Magdó, I.; Müller, M.; Robben, U.; Védova, C. D.; Hildebrandt, P.; Mark, F. J. *J. Phys. Chem. B* **2000**, *104*, 10885.
(92) Gittins, C. M.; Rohlfing, E. A.; Rohlfing, C. M. *J. Chem. Phys.* **1996**, *105*, 7323.
(93) Goodpaster, J. V.; Harrison, J. F.; McGuffin, V. L. *J. Phys. Chem. A* **1998**, *102*, 3372.
(94) Frisch, M. J.; Trucks, G. W.; Schlegel, H. B.; Scuseria, G. E.; Robb, M. A.; Cheeseman, J. R.; Zakrzewski, V. G.; Montgomery, J. A.; Stratmann, R. E.; Burant, J. C.; Dapprich, S.; Millam, J. M.; Daniels, A. D.; Kudin, K. N.; Strain, M. C.; Farkas, O.; Tomasi, J.; Barone, V.; Cossi, M.; Cammi, R.; Mennucci, B.; Pomelli, C.; Adamo, C.; Clifford, S.; Ochterski, J.; Petersson, G. A.; Ayala, P. Y.; Cui, Q.; Morokuma, K.; Malick, D. K.; Rabuck, A. D.; Raghavachari, K.; Foresman, J. B.; Cioslowski, J.; Ortiz, J. V.; Stefanov, B. B.; Liu, G.; Liashenko, A.; Piskorz, P.; Komaromi, I.; Gomperts, R.; Martin, R. L.; Fox, D. J.; Keith, T.; Al-Laham, M. A.; Peng, C. Y.; Nanayakkara, A.; Gonzalez, C.; Challacombe, M.; Gill, P. M. W.; Johnson, B. G.; Chen, W.; Wong, M. W.; Andres, J. L.; Head-Gordon, M.; Replogle, E. S.; Pople, J. A. Gaussian 98; Revision A.7.; Gaussian, Inc.: Pittsburgh, PA, 1998.
(95) Horng, M. L.; Gardecki, J. A.; Papazyan, A.; Maroncelli, M. *J. Phys. Chem.* **1995**, *99*, 17311.
(96) Reynolds, L.; Gardecki, J. A.; Frankland, S. J. V.; Horng, M. L.; Maroncelli, M. *J. Phys. Chem.* **1996**, *100*, 10337.
(97) Xu, Q.-H.; Scholes, G. D.; Yang, M.; Fleming, G. R. *J. Phys. Chem. A* **1999**, *103*, 10348.
(98) Fornasiero, D.; Grieser, F. *J. Chem. Soc., Faraday Trans.* **1990**, *86*, 2955.
(99) Becker, R. S.; Singh, I. S.; Jackson, E. A. *J. Chem. Phys.* **1963**, *38*, 2144.
(100) Shinohara, H.; Yamakita, Y.; Ohno, K. *J. Mol. Struct.* **1998**, *442*, 221.
(101) McHale, J. L. *Acc. Chem. Res.* **2001**, *34*, 265.
(102) Karpovich, D. S.; Blanchard, G. J. *J. Phys. Chem.* **1995**, *99*, 3951.
(103) Larsen, D. S.; Ohta, K.; Xu, Q.-H.; Cyrier, M.; Fleming, G. R. *J. Chem. Phys.* **2001**, *114*, 8008.
(104) Ohta, K.; Larsen, D. S.; Yang, M.; Fleming, G. R. *J. Chem. Phys.* **2001**, *114*, 8020.
(105) Xu, Q.-H.; Ma, Y.-Z.; Fleming, G. R. submitted.
(106) Trebino, R.; DeLong, K. W.; Fittinghoff, D. N.; Sweetser, J. N.; Krumbügel, M. A.; Richman, B. A.; Kane, D. J. *Rev. Sci. Instrum.* **1997**, *68*, 3277.
(107) Homoelle, B. J.; Edington, M. D.; Diffey, W. M.; Beck, W. F. *J. Phys. Chem. B* **1998**, *102*, 3044.
(108) Harvey, S. C.; Hoekstra, P. *J. Phys. Chem.* **1972**, *76*, 2987.
(109) Barrash-Shiftan, N.; Brauer, B.; Pines, E. *J. Phys. Org. Chem.* **1998**, *11*, 743.
(110) Jimenez, R.; Fleming, G. R.; Kumar, P. V.; Maroncelli, M. *Nature* **1994**, *369*, 471.